



1 **Local artifacts in ice core methane records caused by**
2 **layered bubble trapping and in-situ production: a multi-**
3 **site investigation**

4

5 **Rachael H. Rhodes** ^{1*}, **Xavier Faïn** ², **Edward J. Brook** ¹, **Joseph R.**
6 **McConnell** ³, **Olivia J. Maselli** ³, **Michael Sigl** ^{3,4}, **Jon Edwards** ¹, **Christo**
7 **Buizert** ¹, **Thomas Blunier** ⁵, **Jérôme Chappellaz** ², **Johannes Freitag** ⁶

8

9 [1] {College of Earth, Ocean and Atmospheric Sciences, Oregon State University,
10 Corvallis OR, USA}

11 [2] {University Grenoble Alpes/CNRS, Laboratoire de Glaciologie et Géophysique de
12 l'Environnement, Grenoble, France}

13 [3] {Division of Hydrologic Sciences, Desert Research Institute, Reno NV, USA}

14 [4] {Laboratory for Radiochemistry and Environmental Chemistry, Paul Scherrer Institut,
15 Villigen, Switzerland}

16 [5] {Centre for Ice and Climate, Niels Bohr Institute, University of Copenhagen,
17 Copenhagen Denmark}

18 [6] {Alfred Wegener Institute, Helmholtz Centre for Polar and Marine Research,
19 Bremerhaven, Germany}

20 [*] {now at Department of Earth Sciences, University of Cambridge, Cambridge, UK}

21

22 Correspondence to: R. H. Rhodes (rhr34@cam.ac.uk)

23



1 **Abstract**

2 Superimposed on the coherent and major atmospheric changes in trace gases revealed by
3 ice core records, local high frequency, non-atmospheric features can now be resolved due
4 to improvements in resolution and precision of analytical techniques. These are signals
5 that could not have survived the low-pass filter effect that firn diffusion exerts on the
6 atmospheric history and therefore do not result from changes in the composition of the
7 atmosphere at the surface of the ice sheet. Using continuous methane (CH₄) records
8 obtained from five polar ice cores, we characterize these non-atmospheric signals and
9 explore their origin. Isolated samples, enriched in CH₄ in the Tunu13 (Greenland) record
10 are linked to the presence of melt layers. Melting can enrich the methane concentration
11 due to preferential dissolution of methane relative to nitrogen, but we find that an
12 additional in-situ process is required to generate the full magnitude of these anomalies.
13 Furthermore, in the all ice cores studied there is evidence of reproducible, decimetre-
14 scale CH₄ variability. Through a series of tests, we demonstrate that this signal is an
15 artifact of layered bubble trapping in a heterogeneous-density firn column; we term this
16 phenomenon ‘trapping noise’. The magnitude of CH₄ trapping noise increases with
17 atmospheric CH₄ growth rate and seasonality of density contrasts, and decreases with
18 accumulation rate. Firn air transport model simulations, accounting for layered bubble
19 trapping, are in agreement with our empirical data. Significant annual periodicity is
20 present in the CH₄ variability of two Greenland ice cores, suggesting that layered gas
21 trapping at these sites is controlled by regular, seasonal variations in the physical
22 properties of the firn.



1 1 Introduction

2 Continuous measurement of ice core methane (CH_4) concentrations utilising laser
3 spectroscopy (Stowasser et al., 2012) is rapidly emerging as a powerful tool in
4 palaeoclimatology, producing highly detailed records of atmospheric methane for the
5 Last Glacial Period (Chappellaz et al., 2013; Rhodes et al., 2015) and Late Holocene
6 (Rhodes et al., 2013). The ability to expediently and precisely measure trace gases in ice
7 cores at centimetre-scale depth resolution also allows us to locally resolve novel, high
8 frequency signals that do not reflect past atmospheric conditions (Faïn et al., 2014;
9 Rhodes et al., 2013) but instead reveal new information about other processes that
10 influence trace gases in ice cores.

11 The processes of diffusive mixing and gradual bubble close-off, which occur in the firm
12 column, cumulatively act as a low-pass filter, removing high frequency atmospheric
13 signals, such as the CH_4 seasonal cycle (Schwander et al., 1993; Trudinger et al., 1997).
14 All polar ice cores therefore yield trace gas records that are smoothed versions of the
15 actual atmospheric history, with the degree of smoothing depending on site conditions,
16 particularly temperature and accumulation rate (Schwander et al., 1997). Although the
17 degree to which any atmospheric signal is damped by the firm is not always well
18 constrained in the past, it can be estimated (Rosen et al., 2014; Spahni et al., 2003).
19 Trace gas signals present at frequencies above those that could be preserved in the face of
20 the natural smoothing cannot represent atmospheric history. If they are present we must
21 assume that they are not related directly to the original atmospheric variation at the
22 surface of the ice sheet.

23 A previous study of Late Holocene Greenlandic ice (North Greenland Eemian Project
24 (NEEM)-2011-S1 ice core) (Rhodes et al., 2013) identified three categories of non-
25 atmospheric CH_4 signals:

26 1) *Infrequent, abrupt CH_4 spikes (20-100 cm depth interval, 35-80 ppb excess*
27 *CH_4) coincident with elevated concentrations of refractory black carbon and ammonium*
28 *(NH_4^+), suggested to be linked to microbial in-situ production. Similar amplitude CH_4*
29 *anomalies, typically coeval with elevated NH_4^+ , were subsequently reported in Greenland*
30 *Ice Sheet Project 2 (GISP2) Holocene ice (Mitchell et al., 2013). The NEEM Community*



1 Members (2013) also implicated biological in-situ production in the much larger
2 amplitude (> 1000 ppb) CH_4 anomalies observed in NEEM ice dating from the last
3 interglacial (Eemian).

4 2) *CH_4 oscillations of > 100 ppb peak-to-peak amplitude through the lock-in zone.*

5 Following Etheridge et al. (1992) it was suggested that the CH_4 variability was related to
6 the mechanism of layered bubble trapping (Fig. 1). Briefly, according to this mechanism,
7 air bubbles in relatively dense layers close off earlier, trapping anomalously old air, and
8 air bubbles in less dense layers close off later, trapping relatively young air. Providing
9 that there is a sustained gradient of change in atmospheric methane across this time span,
10 the air bubbles in adjacent layers will contain different concentrations of methane.
11 Mitchell et al. (2015) quantified this phenomenon in samples from the lock-in zone of the
12 West Antarctic Ice Sheet (WAIS)-Divide ice core and developed a parameterisation for
13 layered bubble trapping in a firm densification model.

14 3) *Quasi-annual scale CH_4 oscillations of 24 ppb peak-to-peak amplitude in the*

15 *mature ice phase.* Such features had only been observed previously at Law Dome
16 (Etheridge et al., 1992). Rhodes et al. (2013) suggested that they could also have resulted
17 from layered bubble trapping. However, small scale CH_4 oscillations were observed
18 throughout the NEEM-2011-S1 CH_4 record, not only during periods of sustained change
19 in atmospheric CH_4 concentration, questioning whether all the resolved variability could
20 be attributed to the layered bubble trapping mechanism.

21 The findings summarised above generate many questions about what factors affect the
22 biological and/or physical mechanisms responsible for the non-atmospheric CH_4 signals
23 in polar glacial ice. For example, is the suspected in-situ production of CH_4 ubiquitous
24 across the Greenland ice sheet? Can similar anomalous signals be detected in Antarctic
25 ice that has a significantly lower impurity loading? How do site temperature,
26 accumulation rate and impurity load affect the high frequency CH_4 variability tentatively
27 linked to layered bubble close-off?

28 These questions are critically important because ice core trace gas records are integral to
29 palaeoclimatology, enabling us to investigate the relationship between atmospheric
30 greenhouse gases and climate prior to the late 20th century. Recent analytical advances in



1 both discrete (Mitchell et al., 2011) and continuous trace gas measurement techniques
2 (Rhodes et al., 2013; Stowasser et al., 2012) have increased data precision and resolution,
3 which is undoubtedly advantageous for palaeoclimate research, but also increases the
4 likelihood of resolving non-atmospheric signals. Avoiding misinterpretation of non-
5 atmospheric signals and therefore having confidence in the fidelity of the atmospheric
6 histories constructed from ice cores requires detailed knowledge of the physical and
7 biological processes that may locally affect trace gas records. This knowledge, acquired
8 from polar ice cores, could also provide hints about how to extract an atmospheric signal
9 from gas measurements performed on non-polar ice cores that are significantly affected by
10 such artifacts (e.g., Hou et al., 2013). Furthermore, by studying non-atmospheric artifacts
11 in ice core gas records we may learn about the physical mechanisms which trap air
12 bubbles in the firn enabling us to improve numerical model parameterisations used to
13 estimate the gas age-ice age difference and the smoothing effect of firn-based processes.
14 Additionally, it may be possible to glean information about biological activity in one of
15 the harshest biomes on Earth (Rohde et al., 2008).

16 This study examines Late Holocene CH₄ records with centimetre-scale resolution from
17 five polar ice cores with contrasting site characteristics (Table 1). Four of the cores are
18 from Greenland and one is from East Antarctica (Fig. S1). Accumulation rate and
19 temperature, the principal factors affecting firn densification rates, vary considerably
20 between the different cores. Concentrations of chemical impurities contained within the
21 ice can also vary by an order of magnitude (Table 1). Here we compare the ultra-high
22 resolution CH₄ records of the five different ice cores to show that the high frequency non-
23 atmospheric signals we previously observed in NEEM-2011-S1 ice are not unique to this
24 site. Furthermore, we demonstrate how several site characteristics influence the
25 frequency and magnitude of non-atmospheric signals.

26

27 **2 Methods**

28 **2.1 Sample description**

29 The ice core samples analysed in this study are listed in Table 1. Archived samples were
30 obtained from NEEM, D4 and North Greenland Ice Core Project (NGRIP). The NEEM



1 section was chosen to extend the existing NEEM-2011-S1 record further back in time.
2 The D4 record extends the NEEM-2011-S1 record forward in time and is from a warmer
3 Greenland site with twice the accumulation rate. The NGRIP samples are from two Late
4 Holocene depth intervals. A new ice core was retrieved from Tunu, NE Greenland,
5 where accumulation rates are about half those of NEEM or NGRIP. Hereafter the Tunu
6 core will be referred to as Tunu13 to avoid confusion with previous drilling projects.
7 Two Tunu13 cores were drilled: the first (Tunu13 Main) extended from the surface to
8 214 m depth and the second (Tunu13 B) from the surface to 140 m depth. The online gas
9 and chemistry records used in this study are predominantly from the Tunu13 Main core
10 with sections of Tunu13 B spliced in where poor core quality of Tunu13 Main core
11 caused deterioration of the records (Table S1). Prior to analysis, the Tunu13 cores were
12 logged at the National Ice Core Laboratory. Bottom depths of bubble-free layers were
13 recorded and top depths were recorded if the layer's width exceeded 4 mm. It was not
14 possible to discriminate visually between bubble-free layers that were melt layers and
15 those that were wind crusts (Orsi et al., 2015). Both are likely to occur as Tunu is a
16 windy site and our field team found melt layers from the 2012 Greenland melt event. The
17 B40 ice core was drilled close to Kohnen Station, Dronning Maud Land, E Antarctica, by
18 the Alfred Wegner Institute and represents the coldest site with lowest impurity loading
19 of the cores featured in this study (Table 1).

20 **2.2 Analytical methods**

21 All the ice cores listed in Table 1 were analysed at the Desert Research Institute, Reno
22 NV, USA, using a continuous ice core melter system with online gas measurements
23 (Rhodes et al., 2015, 2013). Chemical concentrations in the liquid were measured
24 simultaneously, as described previously (McConnell et al., 2007, 2002).

25 An optical feedback cavity enhanced absorption spectrometer (SARA, developed at
26 Laboratoire Interdisciplinaire de Physique, University Grenoble Alpes, Grenoble, France)
27 (Morville et al., 2005) was used to analyse methane—the same instrument as used by
28 Rhodes et al. (2013) and Faïn et al. (2014). The system response time (t_{90}) was 109
29 seconds, equivalent to 9.4–12.3 cm, depending on the melt rate used for each ice core
30 (Table S1). Methane data were corrected for dissolution in the melted ice core sample



1 following methods described previously (Rhodes et al., 2013). Some system parameters,
2 such as melt rate, varied between ice cores to ensure the best compromise between
3 measurement efficiency and resolution (mainly in liquid phase) and different solubility
4 corrections are used to account for this (Table S1). Allan variance tests performed on
5 measurements of synthetic sample (standard gas mixed with degassed water) suggested
6 an optimal integration time > 1000 s. However, to maximise depth resolution we used an
7 integration time of 5 s, for which Allan variance tests suggest an internal precision of 1.7
8 ppb (2σ).

9 To limit entry of ambient air into the analytical system as breaks in the core were
10 encountered, ice was removed at any angled breaks to obtain a planar surface on which
11 the next ice stick could sit squarely. This resulted in some short sections of data loss.
12 Methane data were manually screened for spikes resulting from ambient air entry at the
13 melterhead (see also section 3.2) because an automated screening algorithm proved too
14 aggressive, resulting in the removal of real variability, as confirmed by discrete CH_4
15 measurements.

16 Methane and chemistry data were mapped onto a depth scale using high resolution (0.1–
17 0.5 Hz acquisition rate) liquid conductivity data and time-depth relationships recorded by
18 system operators. A constant melt rate for each metre length of core is assumed. Depth
19 scale uncertainties are estimated to be ± 2 cm (2σ). The ice and gas age scales used for
20 each ice core are listed in Table 1.

21 For comparison, discrete samples from the Tunu13 ice core were analysed at Oregon
22 State University for methane concentration and total air content. Minor adjustments to
23 the methods of Mitchell et al. (2011) are described in the Supplementary Material.
24 Twenty-four ~ 15 cm depth sections were analysed at 6 cm resolution. External precision
25 of these data, estimated as pooled standard deviation of 34 duplicate sample sets, is 3.1
26 ppb for CH_4 and $0.002 \text{ cm}^3 \text{ STP g}^{-1}$ ice for total air content (1σ).

27 **2.3 Firn air transport models**

28 We compare our empirical data to theoretical model predictions of CH_4 concentrations in
29 closed bubbles resulting from layered gas trapping produced by the Center for Ice and
30 Climate (CIC), Copenhagen, firn air transport model (Buizert et al., 2012), with



1 additional parameterisation of stochastic gas trapping related to local density variability
2 (Mitchell et al., 2015). All experiments are run for the WAIS Divide ice core site
3 because high resolution local density data are available, as well as firn air sample data
4 needed to calibrate the diffusivity profile in the open pores. To accurately capture the
5 influence of layered bubble trapping model simulations are performed at 1 cm vertical
6 resolution. Further details on modeling centimetre-scale air occlusion are provided by
7 Mitchell et al. (2015). The model simulations for the WAIS Divide ice core site can be
8 compared to Greenland ice core sites because the site conditions, particularly temperature
9 and accumulation rate, the principal factors to influence densification are relatively
10 similar (Table 1).

11 We use an additional model, the OSU firn air transport model (Buizert et al., 2012),
12 adapted for palaeo-applications (Rosen et al., 2014) to estimate the smoothing effect that
13 diffusion in the firn has on the CH₄ atmospheric history at each ice core site (Fig. S2).

14

15 **3 Results and discussion**

16 **3.1 Integrity of the atmospheric CH₄ history from ice cores**

17 Multi-decadal scale atmospheric CH₄ variability, previously observed in Law Dome DSS
18 (MacFarling Meure et al., 2006), WAIS Divide (Mitchell et al., 2011), GISP2 (Mitchell et
19 al., 2013) and NEEM-2011-S1 (Rhodes et al., 2013), is faithfully replicated in all the ice
20 cores analysed in this study (Fig. 2). The multi-decadal signals recorded in each core
21 vary in amplitude because the original atmospheric signal has been smoothed to a
22 different extent at each site by firn-based processes. As expected, the low accumulation,
23 cold, East Antarctic core B40 exhibits the most extreme firn-based smoothing (orange
24 line), and the Tunu13 record (green line) shows significant signal damping compared to
25 NGRIP (purple line) due to the lower accumulation rates at Tunu. A future study will
26 focus on the deconvolution of these ice core CH₄ records to generate a consistent
27 atmospheric CH₄ history (Martinerie in prep.). The estimated gas age distribution width
28 at close-off depth for present-day conditions at each ice core site ranges from 14 yr at D4
29 to 65 yr at B40 (Table 1). Atmospheric signals of a shorter period than the gas age



1 distribution width are unlikely to be resolved with their full amplitude in the ice core
2 record.

3 **3.2 Potential in-situ CH₄ production and melt layers**

4 The continuous CH₄ records of all the ice cores analysed contained a high frequency
5 component superimposed on the coherent atmospheric signals shown in figure 2. For this
6 study it was particularly challenging to confidently distinguish between isolated
7 anomalously high CH₄ spikes present in-situ and those resulting from contamination by
8 ambient air. Forest fire haze over Reno during the analytical campaign meant that it was
9 not possible to rely on the absence of a carbon monoxide (CO) signal as indicative of
10 ambient air entry, as has previously been the case (Rhodes et al., 2013). This problem
11 was compounded by poor core quality (high break density, Table S1) in some core
12 sections. However, in a limited number of cases, discussed below, we were able to
13 distinguish between ambient air contamination and in-situ CH₄ signals.

14 Discrete CH₄ measurements performed on Tunu13 ice provided useful information
15 concerning isolated in-situ CH₄ spikes. The CH₄ concentrations of 5 of the 146 discrete
16 samples analysed (Table 2) were anomalously high, between 15 and 80 ppb greater than
17 adjacent samples. The elevated CH₄ samples also had relatively low air content values of
18 0.0847–0.0970 cm³ STP/g ice compared to median of 0.1002 cm STP/g ice (Table 2),
19 negating the possibility of sample contamination by an ambient air leak during analysis.
20 The five anomalous samples were all located within 2.5 cm of bubble-free layers logged
21 during processing (Figs. 3A, 3F-H, Table S2). We therefore hypothesize that these
22 bubble-free layers are melt layers. Melt layers in an ice core may give rise to
23 anomalously high CH₄ values because a) the solubility of CH₄ is greater than that of bulk
24 air, and/or b) of the possibility of enhanced microbial activity (Campen et al., 2003;
25 NEEM community members, 2013).

26 The CH₄ concentration and air content of each of these discrete samples represent a
27 mixture of air from standard bubbly ice and air from a melt layer. Each discrete sample
28 typically spanned 6 cm of ice core depth and, by comparison, the melt layers in the
29 Tunu13 cores were very thin, typically spanning < 5 mm depth. Given that we know the
30 dimensions of each sample and the proportion of the sample volume occupied by the melt



1 layer, we can estimate the CH₄ concentration in the melt layer itself (Table 2). We
2 assume that the air content of each melt layer is $0.0095 \pm 0.0037 \text{ cm}^3 \text{ STP g}^{-1} \text{ ice}$ (1 σ
3 uncertainty, $n = 12$), which is the value measured at Oregon State University on melt
4 layer samples (from the 2012 melt event) collected at Summit, Greenland. Estimated
5 melt layer CH₄ concentrations range from 1829 (+704/-310) ppb to 6355 (+3585/-1574)
6 ppb, equivalent to 2.5–8.6 fold the atmospheric CH₄ concentrations at the time of melt
7 layer formation (Table 2). We then calculate the predicted CH₄ concentration of the melt
8 layers if dissolution of CH₄ from the atmosphere in liquid water reached equilibrium
9 (Table 2). Methane becomes relatively enriched in liquid water that is in equilibrium
10 with the atmosphere because methane is more soluble than nitrogen. The predicted
11 equilibrium CH₄ concentrations are all significantly higher than our estimated melt layer
12 concentrations, suggesting that another process, in addition to dissolution, must
13 contribute to the enrichment of CH₄ in melt layers. Our findings therefore support those
14 of the NEEM Community Members (2013), who found elevated CH₄ concentrations in
15 excess of Henry's Law predictions across a melt layer in the Dye-3 (Greenland) ice core,
16 and also those of Campen et al. (2003), who measured anomalously high CH₄ values that
17 could not be explained by dissolution effects alone. We note that in this study we had to
18 infer the CH₄ concentration of the melt layer because we were not able to obtain a sample
19 of pure melt layer, and the CH₄ values we estimate are relatively uncertain.

20 In light of this apparent link between anomalously high CH₄ concentrations and melt
21 layers in Tunu13 ice, we re-examined the continuous CH₄ data and identified a further 14
22 bubble-free layers, coincident in depth with anomalous CH₄ spikes, that we assume are
23 melt layers (Table S2). The onset of these events can be extremely abrupt, making them
24 appear similar to ambient air contamination. 12 bubble-free layer depths had no
25 continuous CH₄ data, usually because data had been removed due to mixing with
26 standard at start/end of a run or because the ice had been removed across a badly-shaped
27 break. The CH₄ record at a further 20 bubble-free layer depths was affected by ambient
28 air contamination. There are also 78 bubble-free layer depths for which the CH₄ record
29 appears anomaly-free, suggesting that many of these observed bubble-free layers are
30 wind crusts, not melt layers. Alternatively, many of these bubble-free layers did not span
31 the entire horizontal area of the 10 cm diameter core and may have not have been



1 included in the 3.4 x 3.4 cm melter stick cut from the core.

2 We investigated the chemical composition (nitrate, refractory black carbon and
3 ammonium concentrations) of the suspected-melt layers with anomalously high CH₄,
4 because these chemical species were associated with isolated CH₄ spikes in the NEEM-
5 S1-2011 ice core (Rhodes et al., 2013) and GISP2 ice core ((Mitchell et al., 2013)
6 ammonium only). In the Tunu13 record, there was no significant difference between
7 chemical concentrations at depths coincident with anomalously high CH₄ linked to melt
8 layers and chemical concentrations at other depths (Fig. S3).

9 **3.3 Lock-in-zone CH₄ variability**

10 Methane concentrations were measured continuously up-core into the lock-in zone for
11 three ice cores: D4, Tunu13 and B40. We observed a marked increase in the amplitude
12 of decimetre-scale variability and a gradual decrease in gas flow to the instrument
13 through the lock-in zone (Fig. S4), similar to results produced by continuous CH₄
14 analysis of the lock-in zones in NEEM-2011-S1 (Rhodes et al., 2013) and WAIS Divide
15 (WDC05A, Mitchell et al. (2015)) ice cores. The sharp increase in the amplitude of high
16 frequency variability by up to 10-fold makes the base of the lock-in zone (close-off
17 depth) easily recognisable in continuous CH₄ data. We estimate the close-off depth to be
18 82 m at D4, 73 m at Tunu13 and 95 m at B40, comparable to values from firn air field
19 campaigns at the latter two sites (Tunu13: Butler et al., 1999; B40: Weiler, 2008). For
20 D4, the continuous CH₄ data appear to encompass the entire lock-in zone; at 68 m depth
21 the high amplitude oscillations cease and CH₄ concentrations stabilise at 1860 ppb, close
22 to the ambient concentrations, which suggests that the air measured by the laser
23 spectrometer at this point was only laboratory air entering the system through the open
24 porosity. Our results therefore suggest that the lock-in depth at D4 is 68 m, 3 m deeper
25 than predicted by the OSU firn air model.

26 Initial examination suggests that the magnitude of lock-in zone CH₄ variability varies
27 significantly between cores (Fig. S4) but it is not possible to quantify the degree of
28 ambient air contamination influencing our lock-in zone measurements, either from
29 laboratory air (~1890 ppb) via inter-connected open porosity or from post-coring bubble
30 closure (Aydin et al., 2010). It is therefore difficult to quantify the influence of time-



1 staggered bubble trapping on lock-in zone CH₄ variability. However, we have reason to
2 believe that the proportion of ambient laboratory air versus air from the closed porosity
3 may be low because continuous CH₄ measurements of WAIS Divide lock-in zone
4 samples conducted using the same analytical system were well replicated by discrete CH₄
5 measurements (see Mitchell et al., 2015 Fig. S5). Furthermore, Mitchell et al. (2015)
6 used $\delta^{15}\text{N}$ of N₂ data measured on the WAIS Divide lock-in zone samples to calculate the
7 proportion of air affected by post-coring bubble closure as $10.6 \pm 6.1\%$; this value should
8 be considered as an upper estimate as the core used in that study was stored for ~ 6 yr
9 prior to analysis.

10 **3.4 High frequency non-atmospheric signals in mature ice**

11 **3.4.1 Observations**

12 In the mature ice phase below the close-off depth we observe significant decimetre-scale
13 variability in the CH₄ records of every ice core analysed. In each case, it is impossible
14 that this high frequency signal could have existed in the atmosphere at the ice sheet
15 surface and survived the low-pass filter action of the firn—the gas age distribution widths
16 (Table 1) are greater than the approximate signal periods. We initially focus in detail on
17 only Tunu13 and B40 because these are the most complete records, with relatively little
18 ice removed prior to analysis and few ambient air entry problems, both factors linked to
19 the number of core breaks (Table S1).

20 A smoothing spline is subtracted from the CH₄ record of each site to effectively remove
21 the atmospheric signal (Fig. 3A&B, Tunu13 shown). The residual CH₄ record contains a
22 high frequency non-atmospheric signal and analytical noise (Fig. 3B). The mean peak-
23 to-peak amplitude (see Supplementary Material) of the residual high frequency CH₄ in
24 the Tunu13 record from 987 to 1870 AD gas age is 5.3 ppb (median is 3.7 ppb) and
25 varies between 2 ppb and 42 ppb. Similar peak-to-peak amplitude and frequency was
26 observed in the continuous CH₄ profile obtained along the NEEM ice core (Chappellaz et
27 al., 2013). It was attributed to analytical system noise, specifically variations in gas
28 permeation across the gas-permeable membrane used to extract gas from the sample
29 stream. Here, we have confidence that we capture a high frequency signal present above
30 the analytical noise in some sections of the record because discrete CH₄ measurements on



1 the Tunu13 core conducted at 6 cm resolution also show substantial variability within
2 each 15 cm depth section. CH₄ concentrations in adjacent samples differ by up to 32 ppb,
3 but more typically by 3.4 ppb, and reproduce some of the decimetre-scale changes
4 resolved by the continuous measurements (Fig. 3C-E). CH₄ oscillations captured by the
5 discrete measurements are larger in amplitude than those in the continuous gas record
6 because the continuous gas analysis system causes more signal smoothing than the
7 discrete analysis (Stowasser et al., 2012) (Table S1, Fig S2). The 5.3 ppb mean peak-to-
8 peak amplitude of this high frequency non-atmospheric signal must therefore be a
9 minimum estimate.

10 A high frequency, non-atmospheric signal in excess of analytical noise is also present in
11 sections of the B40 continuous CH₄ record and it is reproducible; we measured replicate
12 ice core sticks on different days and were able to resolve very similar decimeter-scale
13 features in ice samples from 114–120 m depth (Fig. 4). The sharp CH₄ troughs at 122.8,
14 122.6, 122.3, 121.3 and 120.2 m are particularly well replicated and highly unlikely to be
15 analytical artifacts. The mean peak-to-peak amplitude of the high frequency non-
16 atmospheric signal in this section of the B40 record is 5.4 ppb (median is 5.1 ppb).

17 **3.4.2 Evidence for layered bubble trapping**

18 Our results demonstrate that the quasi-annual variability previously observed in the ice
19 phase of the NEEM-2011-S1 core (Rhodes et al., 2013) is not unique to NEEM or to
20 Greenlandic ice. The question now is: what causes it? If it is an artifact of layered
21 bubble trapping, as speculated for NEEM-2011-S1, the observed decimetre-scale
22 variability should respond in a predictable way to several factors that vary over time and
23 between ice core sites. We therefore systematically examine our empirical data to assess
24 the influence of each factor and judge whether any relationship is consistent with the
25 mechanism of layered bubble trapping.

26 *- Atmospheric CH₄ growth rate*

27 Our conceptual model of layered bubble trapping predicts that the difference in CH₄
28 concentration between adjacent layers (ΔCH_4) should increase with the CH₄ concentration
29 gradient in the firn column, which is dictated by the atmospheric CH₄ growth rate (Fig.
30 1). We can clearly observe this relationship in the Tunu13 record; amplitudes of the



1 decimetre-scale CH₄ oscillations are greatest when the atmospheric CH₄ concentration
2 shows a sustained trend of increase or decrease, particularly during the steep post-
3 Industrial Revolution CH₄ rise and the growth and decay in atmospheric CH₄
4 concentrations associated with the prominent CH₄ oscillation centered on 1550 AD (Fig.
5 3B).

6 To explore this relationship quantitatively, we compare the CH₄ growth rate to the
7 standard deviation (σ) of the high frequency CH₄ residual (data minus spline, as Fig. 3B)
8 for moving windowed sections of the Tunu13 record. Windows are 40 yr in length and
9 are calculated every 10 yr interval. Strong linear relationships between CH₄ growth rate
10 and the magnitude of high frequency variability are revealed for atmospheric CH₄ growth
11 and decay rates > 0.4 ppb yr⁻¹ (Fig. 5E). The gradients of the linear relationships are
12 similar in both cases ($7\text{--}8$ ppb σ -CH₄/ppb yr⁻¹ growth rate). At low growth rates (< 0.4
13 ppb yr⁻¹) σ -CH₄ values reflect the analytical precision of 1.7 ppb. The observation that σ -
14 CH₄ only increases beyond analytical noise at growth rate > 0.4 ppb yr⁻¹ heavily
15 implicates the mechanism of layered bubble trapping as the cause of the high frequency
16 CH₄ signal because it requires sustained trend of change in atmospheric concentration to
17 produce CH₄ artifacts (Fig. 1). We therefore define high frequency non-atmospheric CH₄
18 variability in excess of analytical noise as “trapping noise”.

19 This analysis was repeated on the high frequency CH₄ residual records from other ice
20 cores: B40, NEEM-2011-S1, D4 and NGRIP (Fig. 5 A-D). For NGRIP, only data from
21 1050–1240 AD and 1774–1860 AD (gas age) were used, the latter with a 10 yr length
22 window to avoid data gaps. For NEEM-2011-S1, data from 1450–1840 AD were used.
23 Any 40 yr time window with a data gap > 5 yr duration was discarded from analysis. We
24 note that the CH₄ growth rate recorded in the ice core is not strictly equivalent to the
25 atmospheric growth rate because firn-based smoothing may have caused some damping
26 of the signal (Fig. 2). The B40 record is significantly affected by firn-based smoothing
27 (Fig. S2), which reduces the growth rate captured by the ice core archive. The B40
28 record is also severely impacted by system-based smoothing (Fig. S2), which damps
29 trapping noise to within range of the analytical noise for much of the record, excepting
30 the section displayed in figure 4. The combination of these two effects destroys any
31 relationship between atmospheric growth rate and amplitude of the high frequency signal



1 (Fig. 5A). There is also little sign of a relationship between growth rate and σ -CH₄ in the
2 NEEM-2011-S1 data (Fig. 5B) and we speculate this is the result of a more aggressive
3 ambient air screening method applied by Rhodes et al. (2013) that may have removed real
4 variability.

5 Results are more encouraging for D4 and NGRIP as both sites exhibit linear relationships
6 between CH₄ growth rate and the magnitude of trapping noise (Fig. 5C&D). Both
7 negative and positive growth rates at NGRIP exhibit the same gradient of change with σ -
8 CH₄. The consistency of results between sites is important for the identification of
9 layered bubble trapping as the mechanism behind the high frequency variability. Further
10 support can be drawn from CIC firm air transport model, which predicts a linear
11 relationship between atmospheric growth rate and the magnitude of CH₄ trapping noise at
12 WAIS Divide (red line, Fig. 5F). When the Tunu13, D4 and NGRIP data are all plotted
13 on the same axes with the WAIS Divide model simulation (Fig. 5F), the gradient of the
14 modeled linear relationship is within the range of gradients of our empirical data from 3
15 different Greenland ice core sites. Clearly, the magnitude of CH₄ trapping noise (σ -CH₄)
16 does not have the same sensitivity to growth rate at all ice core sites; another factor is
17 influencing CH₄ variability, as we explore below.

18 For completeness we note that physics tells us that there can still be a tiny layered bubble
19 trapping signal at zero growth rate due to the effect of gravity. As CH₄ is lighter than air,
20 gravity reduces the CH₄ concentration with depth relative to the concentration in the
21 atmosphere. Thus at zero growth rate there is still a CH₄ gradient in the firm that can
22 result in the generation of trapping noise via layered gas occlusion. This also means that
23 at positive atmospheric growth rates, the gravitational gradient must be overcome in order
24 to generate CH₄ oscillations related to layering. This is why the modeled WAIS Divide
25 growth rate vs. σ -CH₄ plot intersects the x-axis at a slightly positive growth rate and σ -
26 CH₄ is predicted to be 0.11 ppb at zero growth rate (Fig. 5F). This effect is an order of
27 magnitude smaller than the analytical noise and is not detectable.

28 - Accumulation rate

29 At a constant atmospheric growth rate, the amplitude of CH₄ trapping noise produced by
30 layered bubble trapping should be determined by the difference in age between the air



1 trapped relatively early compared to younger air trapped relatively late (t_2 minus t_1 on
2 Fig. 1). One factor that will affect how quickly an adjacent layer is closed off is
3 accumulation rate (A)—more new snow accumulation will cause layers to spend less time
4 in the firn column reducing the time interval over which layered bubble trapping can
5 occur. We test this hypothesis by comparing the magnitude of CH_4 trapping noise in ice
6 cores with different accumulation rates (Fig. 6A&B). Comparison is performed for two
7 discrete time periods (gas age) for which we have good quality (continuous and above
8 analytical noise) CH_4 residual data from three cores, and we assume all three sites
9 experienced the same atmospheric growth rate. As expected, there is a significant
10 decrease in $\sigma\text{-CH}_4$ with increasing accumulation rate for the 1770–1900 AD time period
11 (Fig. 7B), but the 1490–1630 AD interval shows shows no trend (Fig. 6A).

12 However, if we adjust the $\sigma\text{-CH}_4$ values of each ice core to compensate for different the
13 smoothing effect of the analytical system, the results from the two time intervals become
14 more consistent (Fig. 6C&D). To perform this adjustment, we assume that the high
15 frequency signal has an annual periodicity and consult the Bode plots generated from
16 switching the analytical system between two gas standards, to determine what fraction of
17 the original amplitude is retained by the system (Fig. S2). The nature of this relationship
18 differs between time slices considered. An inverse relationship between $\sigma\text{-CH}_4$ and
19 annual layer thickness is identifiable for the 1490–1630 AD interval and a power law fit
20 is applied, but a linear relationship would also be applicable here. A power law
21 relationship is identifiable between annual layer thickness and $\sigma\text{-CH}_4$ for the 1770–1900
22 AD time period, which has the greatest range of annual layer thickness and $\sigma\text{-CH}_4$ values.
23 These corrected data suggest that, at a fixed growth rate, an inverse relationship exists
24 between accumulation rate and the magnitude of CH_4 variability ($\sigma\text{-CH}_4$). This is how
25 we would expect CH_4 trapping noise to respond to accumulation rate.

26 CIC firn air transport model simulations for WAIS Divide exhibit a similar power law
27 relationship to the empirical data, whereby $\sigma\text{-CH}_4$ is proportional to $1/A^{1.47}$. The slope is
28 the result of two separate effects. First, increasing A decreases the time adjacent layers
29 spend in the firn column, which by itself should cause CH_4 trapping noise to scale as $1/A$.
30 Second, at increased A the advective gas transport in the open pores is enhanced, and this
31 reduces the CH_4 gradient down the firn column. If bubbles are then trapped over the



1 same depth range, the amplitude of CH₄ variability will be reduced, and this effect
2 appears to scale as $1/A^{0.47}$ in the firm model. An important caveat is that the firm model
3 assumes no change in the firm density profile with changing accumulation rate, which is
4 probably unrealistic. However, the model does appear to capture a response of CH₄
5 trapping noise to accumulation rate that is roughly comparable to that observable in the
6 real-world data.

7 - *Firn density layering*

8 Another factor that should influence the amount of time that passes between early and
9 late bubble closure is the degree of contrast between the physical properties of firn in
10 adjacent layers. There is no doubt that the physical properties of firn ultimately control
11 when a bubble is occluded, or a layer is completely sealed off. The relative importance
12 of local density variability, firn microstructure, permeability and/or porosity in this
13 process is actively debated. The traditional interpretation of density as the principal
14 influence on bubble occlusion is being challenged (Gregory et al., 2014). However, we
15 concentrate on the potential influence of local density variability in this section.

16 The controls on density layering in the firn are poorly understood, but a recent study
17 suggests that variability near the firn-ice transition is higher at warmer, high
18 accumulation sites (Hörhold et al., 2011). It is difficult to test the effects of density
19 layering because we do not have the high resolution density information required to do
20 so. However, we can use the CIC firn air transport model, which utilises high resolution
21 density data for the WAIS Divide ice core, to make a prediction. In these simulations, we
22 define the density layering to be $\rho_{\text{layer}} = \rho - \langle \rho \rangle$ with the local firn densities (ρ) as given
23 by the high resolution measurements, and the bulk density ($\langle \rho \rangle$) as given by a spline fit
24 to those data. We then run the model several times with a density profile that equals $\rho =$
25 $\langle \rho \rangle + \alpha \rho_{\text{layer}}$. By varying the scaling parameter α between 0 and 1.6 we can effectively
26 control the magnitude of the firn density layering. As we would expect, no high
27 frequency CH₄ trapping noise is produced in the absence of density layering ($\alpha = 0$) (Fig.
28 S5). When the magnitudes of the local density anomalies are halved ($\alpha = 0.5$), the
29 amplitude of the trapping noise decreases slightly more than 2-fold from 7.3 ppb to 3.2
30 ppb. This effect is minor compared to that of accumulation rate or atmospheric growth



1 rate. However, it may explain why interior Antarctic sites, like B40, which have less
2 pronounced seasonality in density at the firn-ice transition compared to coastal Antarctic
3 or Greenland locations (Hörhold et al., 2011) may show only moderate trapping noise
4 despite the extremely low accumulation rates.

5 **3.5 Layered gas trapping mechanism**

6 Having established that the high frequency CH₄ signal we observe in all the ice cores in
7 this study shows characteristics consistent with the mechanism of layered gas trapping
8 (Fig. 1), we are able to discern aspects of this physical process.

9 First, the CH₄ trapping noise measured for the different ice core sites allows us to
10 estimate the age difference between the air samples trapped in adjacent layers (t_2 minus t_1
11 on Fig. 1). High frequency CH₄ residual data, corrected for system smoothing effects
12 (section 3.4.2) from the 1810–1860 AD time interval, which has an atmospheric growth
13 rate of 1.5 ppb yr⁻¹ (in D4—the least susceptible record to firn-based smoothing of the
14 atmospheric signal), suggest a gas age difference between adjacent layers of 23 yr at
15 Tunu13, 2.4 yr at D4 and 5 yr at NGRIP. These values can be compared to previously
16 published estimates of 10 yr for WAIS Divide (Mitchell et al., 2015), 12 yr for NEEM-
17 2011-S1 (Rhodes et al., 2013) and 2 yr for Law Dome (Etheridge et al., 1992).
18 Unsurprisingly, the gas age difference is greater at lower accumulation sites. To negate
19 the issue of smoothing associated with the analytical system, we also consider Tunu13
20 discrete measurements, which show a maximum oscillation of 32 ppb amplitude at an
21 atmospheric growth rate of 1.5 ppb yr⁻¹ (Fig. 3C). The age difference between layers in
22 this case would be 21 yr, which is very close to the estimate above.

23 Second, the frequency of CH₄ oscillations resulting from layered bubble trapping should
24 reflect the difference in depth, and therefore also ice age (not the age of the gas trapped
25 inside the bubbles, as discussed above) between adjacent firn layers where bubbles are
26 closed off at different times. To test this with our ice core data we perform multi-taper
27 method (MTM) spectral analysis of the Tunu13, D4, NGRIP and B40 CH₄ records (Fig.
28 7). Spectral analysis is performed in the ice age domain because we believe that physical
29 properties of the firn/ice phase are ultimately responsible for the high frequency artifacts
30 recorded in the gas phase at the same depth. Prior to analysis each 40 yr window of data



1 (as section 3.4.2) is interpolated to an even ice age spacing that is twice the median
2 sample spacing and any windows with data gaps > 2 yr are ignored. We then averaged
3 the MTM spectra produced to generate mean spectra for sections of the record with
4 relatively high or low growth rate, or in the case of D4, sections of the record
5 encompassing mature ice or some firn.

6 Sections of the Tunu13 record with CH_4 growth rates $> 0.4 \text{ ppb yr}^{-1}$ exhibit spectral peaks
7 at 1 yr period in ice age domain and the averaged spectra for growth rates $> 0.4 \text{ ppb yr}^{-1}$
8 has a significant 1 yr periodicity (95% confidence) (Fig. 7). By contrast, sections of the
9 Tunu13 record with growth rates $< \pm 0.4 \text{ ppb yr}^{-1}$ show no significant periodicity. The
10 high accumulation Greenland ice core D4 shows an annual periodicity in CH_4 , but it only
11 becomes significant when data from the lock-in zone are included (Fig. 7). NGRIP
12 shows small spectral peaks at 1yr period for 2 (out of 4) time windows with growth rates
13 $> 0.2 \text{ ppb yr}^{-1}$ but the peak in the averaged spectrum is not significant (Fig. 7). Again,
14 NGRIP data sections with growth rates $< 0.2 \text{ ppb yr}^{-1}$ exhibit no periodicity. No
15 significant periodicity is resolved in the B40 high frequency residual CH_4 record,
16 potentially because any annual signal has been removed by analytical system smoothing.

17 The significant annual periodicity resolved in the Tunu13 and D4 during periods of
18 relatively high growth rates strongly suggests that the mechanism of layered bubble
19 trapping is linked to regular, seasonal variations in the physical properties of the firn
20 pack, over a wide range of Greenland ice core site conditions. The quasi-annual high
21 frequency signal observed in mature NEEM-2011-S1 ice (Rhodes et al., 2013) could also
22 be added to this list. We note that even if there is some ambient air contamination of
23 lock-in zone CH_4 measurements, the wavelength of the CH_4 oscillations in the lock-in
24 zone should reflect the depth spacing of alternating layers with contrasting ratios of open
25 to closed porosity, and therefore relatively more or less contamination. The sharp,
26 significant spectral peak at a 1 yr periodicity (Fig. 7) therefore suggests a strong seasonal
27 contrast in the physical properties of firn at this site. It is possible that several different
28 physical properties influence layered bubble occlusion in addition to or instead of local
29 density variability (Gregory et al., 2014) but it is now understood that the sign of relative
30 density contrast between seasonal snow layers switches over before the firn-ice transition
31 is reached so that initially less dense summer layers densify faster and eventually become



1 denser than neighbouring winter layers (Freitag et al., 2004; Gerland et al., 1999; Hörhold
2 et al., 2011). Our results could therefore suggest that the density variations preserved at
3 the firn-ice transition maintain an imprint of annual variability that is strong enough to
4 produce regular layering in the firn, resulting in CH₄ trapping noise with a significant
5 annual periodicity.

6 It is still not clear precisely how and why layering in polar firn evolves with depth and
7 time in the way that it does. Hörhold et al. (2012) suggested that “impurities” which
8 exhibit an annual cycle in concentration may act to promote densification by softening
9 the seasonal firn layers. Hörhold et al. (2012) reported positive correlations between
10 soluble calcium (Ca²⁺) concentration and local density but their choice of Ca²⁺ was not
11 supported by any physical causal link between Ca²⁺ and densification rate. Subsequent
12 work suggested that chloride (Cl⁻) and fluoride (F⁻) were more likely candidates to drive
13 densification (Fujita et al., 2014), in conjunction with seasonal variations in
14 microstructure. Fujita et al. (2014) refer to early experiments which detail how
15 substitution of Cl⁻ and F⁻ into the ice lattice promotes dislocations and causes a softening
16 effect (Jones, 1967; Nakamura and Jones, 1970). In Greenland ice, Cl⁻ concentrations
17 peak in winter and F⁻ concentrations peak slightly later, in early spring, coincident with
18 Ca²⁺.

19 Our data cannot resolve this issue, but we can use the chemical concentrations measured
20 as a proxy for local density, assuming that winter/spring chemical species like Ca and Cl
21 are enriched in the relatively dense layers. In the Tunu13 ice core, concentrations of Ca
22 and Cl show significant negative correlation ($p < 0.05$) with CH₄ anomalies when growth
23 rates are positive (Fig. 8). A similar relationship is observable for the short section of the
24 B40 core with significant CH₄ trapping noise, using Na in place of Cl in this instance
25 because it is easier to measure at very low concentrations (Fig. 4B). These observations
26 confirm the seasonality of layered gas trapping that we have assumed—Ca and Cl-rich,
27 dense, layers trap air earlier, preserving a relatively low CH₄ concentration when
28 atmospheric CH₄ is increasing, and vice versa. Correlation between impurity levels in the
29 ice and CH₄ anomalies does not signify a causal link between them. It makes sense that
30 the correlation between chemistry and CH₄ is stronger at high growth rates because the
31 trapping noise produced at these times has relatively a high amplitude and an annual



1 periodicity. What is more interesting is that the sign of the correlation coefficient
2 between Ca or Cl and the high frequency CH₄ signal switches when CH₄ growth rate is
3 negative rather than positive (Fig. 8). When atmospheric CH₄ is decreasing, a Ca-Cl-rich
4 layer that closes off early will trap air with a relatively high CH₄ concentration. This is
5 an important final piece of evidence to attribute the high frequency CH₄ signal in ice
6 cores to layered bubble trapping.

7

8 **4 Summary**

9 **4.1 Methane artifacts related to melt layers**

10 We have demonstrated that narrow, isolated peaks in CH₄ concentration in the Tunu13 ice
11 core record are located at depths coincident with bubble-free layers assumed to be melt
12 layers. CH₄ measurements on discrete ice samples enabled us to confidently link melt
13 layers and CH₄ enrichment, circumventing the complication of potential ambient air
14 contamination from the continuous-flow system. These findings contrast with our
15 previous study (Rhodes et al., 2013), in which we found no melt layers associated with
16 anomalous CH₄ signals in the NEEM-2011-S1 core, but are in agreement with published
17 data showing trace gas enrichment across melt layers in the Dye 3 (Greenland) ice core
18 (NEEM community members, 2013; Neftel et al., 1983). Furthermore, we confirm this
19 and earlier work (Campen et al., 2003) suggesting that dissolution of CH₄ in the liquid
20 phase cannot account for the full magnitude of CH₄ enrichment in melt layers,
21 suggesting, but not proving, that biological activity may be in part responsible for the
22 observed CH₄ enrichment. In this respect our results complement the findings of the
23 NEEM Community Members (2013) and we suggest that if significantly older ice had
24 been sampled at Tunu13, we may have observed greater CH₄ enrichment in excess of
25 equilibrium at melt layer depths. Additionally, we find no significant relationships
26 between the anomalously high CH₄ levels at melt layer depths and concentrations of
27 chemical species (NH₄⁺, rBC or NO₃⁻) present in the ice phase of the Tunu13 ice core.

28 In the absence of a systematic, reliable methodology to confidently distinguish between
29 elevated in-situ CH₄ signals and ambient air contamination, this study can only contribute
30 limited information regarding the potential for biological in-situ production of methane in



1 polar ice at this stage. The implications of biological in-situ production in polar ice are so
2 far-reaching (Prisco and Hand, 2010) that it deserves further investigation by a dedicated
3 multi-disciplinary project. Continuous trace gas analysis is an effective tool for screening
4 cores to identify depth ranges with interesting signals but further analysis including
5 $\delta^{13}\text{CH}_4$, organic species and meticulous microbiological characterisation are needed.

6 **4.2 Methane artifacts resulting from layered bubble trapping**

7 This study uses high resolution continuous CH_4 data from five Late Holocene ice cores to
8 demonstrate that layered bubble trapping causes high frequency (decimetre-scale)
9 oscillations in the CH_4 record of mature ice from both Antarctica and Greenland when
10 there is a sustained positive or negative trend in atmospheric growth rate. These features,
11 deemed trapping noise, have been reproduced by discrete and continuous CH_4
12 measurements and cannot reflect atmospheric history because firn-based smoothing
13 processes would have removed them.

14 Using empirical data supported by a firn air transport model simulations we demonstrate
15 that the CH_4 trapping noise responds in predictable ways to atmospheric growth rate and
16 site specific factors, particularly accumulation rate. The amplitude of the CH_4 trapping
17 noise increases with atmospheric growth rate and seasonal density contrasts, and
18 decreases with accumulation rate. The layered bubble trapping signal in two Greenland
19 ice core records has a significant annual periodicity, demonstrating that the seasonal
20 contrasts in firn physical properties which develop above the firn-ice transition are
21 regular and uniform enough to generate periodic CH_4 artifacts.

22 **5 Implications**

23 **5.1.1 For future ice core trace gas analysis**

- 24 • As resolution and precision of analytical techniques improve, analysts need to be
25 aware that high frequency signals, not related to past atmospheric variability, are
26 present in ice core trace gas records due to enrichment associated with melt layers and
27 variability related to layered bubble trapping.
- 28 • Careful choices regarding discrete sample size and dimension, and post-processing of
29 continuous data sets are required to avoid misinterpretation. Analysts should



1 integrate trace gas data over multiple annual layers to smooth out trapping noise and
2 anticipate isolated anomalous CH₄ signals at sites where surface melt is possible.
3 This is especially relevant for studies of the inter-polar gradient (e.g., Mitchell et al.,
4 2013) because the absolute concentrations are so important to the conclusions
5 reached.

6 • The magnitude of CH₄ trapping noise within an ice core record or in a time slice can
7 be predicted using a firm air transport model adapted for the purpose (Mitchell et al.,
8 2015), provided information about the local density variability at the site is known.
9 For Holocene ice, density information from the firm could plausibly be extrapolated to
10 the deeper ice, but it is unlikely that density variability was similar under widely
11 different climatic conditions. If variability in chemical concentrations or impurities
12 recorded in the ice phase could somehow be interpreted as a proxy for local density
13 variability, this could help to inform modeling efforts. This study presents only an
14 incremental step towards utilising chemistry records in this way.

15 • The layered bubble trapping process has the effect of broadening the gas age
16 distribution of the air trapped in the closed porosity, if the air is sampled across
17 several adjacent layers. This effect increases with decreasing accumulation rate as the
18 time interval between bubble closure in adjacent layers is increased. However, this
19 effect is a relatively minor contribution to the magnitude of the gas age distribution at
20 all but the lowest accumulation sites.

21 **5.1.2 For our understanding of gas trapping**

22 • Our empirical data suggest that layered gas trapping is driven by highly regular
23 (seasonal) variations in the physical properties of layered firm. Whether local density
24 or some other closely-related property is primarily responsible for driving this
25 variability in bubble occlusion is not clear.

26 • We do not find evidence of major ‘sealing layers’, vast in their horizontal extent,
27 which would prevent vertical diffusion of trace gases in the diffusive column. Rather,
28 the regularity of the high frequency CH₄ signal suggests that even as denser layers are
29 closed off at shallower depths in the firm column, vertical diffusion down the firm
30 column is maintained. This could be via cracks in dense layers or via channels of



1 open porosity tracking around isolated dense “lenses”. A similar conclusion was
2 reached by Keegan et al. (2014) in their exploration of how ice layers impact air
3 movement in the NEEM firn.

4 An open question generated by this study is: Why do the high frequency oscillations in
5 CH₄ concentration increase sharply in amplitude at the base of the lock-in zone? The
6 findings of Mitchell et al. (2015) suggest that contamination from ambient air is relatively
7 low in continuous data from the lock-in zone, not enough to account for the 10-fold
8 amplitude increase. So, if CH₄ variability in the lock-in zone and in the mature ice phase
9 are both related to layered bubble trapping, what causes the discontinuity? It may be that
10 the only way to resolve this question is to devise a way to eliminate the possibility of
11 contamination with ambient air, perhaps by analysing trace gases across the lock-in zone
12 to mature ice transition in-situ.

13

14 **Acknowledgements**

15 This work was supported by US National Science Foundation (NSF) grants 1204172,
16 0944552, 1204176 and 0909541 and NSF Partnerships in International Research and
17 Education (PIRE) Grant 0968391. This work was additionally supported by the French
18 ANR program RPD COCLICO (ANR-10-RPDOC-002-01) and received funding from
19 the European Research Council under the European Community’s Seventh Framework
20 Program FP7/2007-2013 Grant Agreement #291062 (project ICE&LASERS). We thank
21 Nathan Chellman, Daniel Pasteris, Larry Layman and Amber Zandanel for laboratory
22 assistance, Nicole Rocco for Summit melt layer measurements, and Julia Rosen for use of
23 OSU firn model. We are very grateful to Beth “Bella” Bergeron for her valuable
24 expertise, leadership and hard work drilling the Tunu13 cores. Our field team received
25 valuable assistance from CH2HILL and Ken Borek Air. The NEEM project is directed
26 by the Centre for Ice and Climate at the Niels Bohr Institute, Copenhagen and the US
27 NSF OPP. It is supported by funding agencies and institutions in Belgium (FNRS-CFB
28 and FWO), Canada (NRCan/GSC), China (CAS), Denmark (FIST), France (IPEV,
29 CNRS/INSU, CEA and ANR), Germany (AWI), Iceland (RannIs), Japan (NIPR), Korea
30 (KOPRI), The Netherlands (NWO/ALW), Sweden (VR), Switzerland (SNF), United



- 1 Kingdom (NERC) and the USA (US NSF, OPP). We are grateful to the North Greenland
- 2 Ice Core Project (NGRIP) for providing samples.



1 References

- 2 Aydin, M., Montzka, S.A., Battle, M.O., Williams, M.B., De Bruyn, W.J., Butler, J.H.,
 3 Verhulst, K.R., Tatum, C., Gun, B.K., Plotkin, D.A., Hall, B.D., Saltzman, E.S.,
 4 2010. Post-coring entrapment of modern air in some shallow ice cores collected
 5 near the firn-ice transition: evidence from CFC-12 measurements in Antarctic firn
 6 air and ice cores. *Atmos Chem Phys* 10, 5135–5144. doi:10.5194/acp-10-5135-
 7 2010
- 8 Buizert, C., Martinerie, P., Petrenko, V.V., Severinghaus, J.P., Trudinger, C.M., Witrant,
 9 E., Rosen, J.L., Orsi, A.J., Rubino, M., Etheridge, D.M., Steele, L.P., Hogan, C.,
 10 Laube, J.C., Sturges, W.T., Levchenko, V.A., Smith, A.M., Levin, I., Conway,
 11 T.J., Dlugokencky, E.J., Lang, P.M., Kawamura, K., Jenk, T.M., White, J.W.C.,
 12 Sowers, T., Schwander, J., Blunier, T., 2014. Corrigendum to ‘‘Gas transport in
 13 firn: multiple-tracer characterisation and model intercomparison for NEEM,
 14 Northern Greenland’’ published in *Atmos. Chem. Phys.*, 12, 4259–4277, 2012.
 15 *Atmos Chem Phys* 14, 3571–3572. doi:10.5194/acp-14-3571-2014
- 16 Buizert, C., Martinerie, P., Petrenko, V.V., Severinghaus, J.P., Trudinger, C.M., Witrant,
 17 E., Rosen, J.L., Orsi, A.J., Rubino, M., Etheridge, D.M., Steele, L.P., Hogan, C.,
 18 Laube, J.C., Sturges, W.T., Levchenko, V.A., Smith, A.M., Levin, I., Conway,
 19 T.J., Dlugokencky, E.J., Lang, P.M., Kawamura, K., Jenk, T.M., White, J.W.C.,
 20 Sowers, T., Schwander, J., Blunier, T., 2012. Gas transport in firn: multiple-tracer
 21 characterisation and model intercomparison for NEEM, Northern Greenland.
 22 *Atmospheric Chem. Phys.* 12, 4259–4277. doi:10.5194/acp-12-4259-2012
- 23 Butler, J.H., Battle, M., Bender, M.L., Montzka, S.A., Clarke, A.D., Saltzman, E.S.,
 24 Sucher, C.M., Severinghaus, J.P., Elkins, J.W., 1999. A record of atmospheric
 25 halocarbons during the twentieth century from polar firn air. *Nature* 399, 749–
 26 755. doi:10.1038/21586
- 27 Campen, R.K., Sowers, T., Alley, R.B., 2003. Evidence of microbial consortia
 28 metabolizing within a low-latitude mountain glacier. *Geology* 31, 231–234.
 29 doi:10.1130/0091-7613
- 30 Chappellaz, J., Stowasser, C., Blunier, T., Baslev-Clausen, D., Brook, E.J., Dallmayr, R.,
 31 Faïn, X., Lee, J.E., Mitchell, L.E., Pascual, O., Romanini, D., Rosen, J.,
 32 Schüpbach, S., 2013. High-resolution glacial and deglacial record of atmospheric
 33 methane by continuous-flow and laser spectrometer analysis along the NEEM ice
 34 core. *Clim Past* 9, 2579–2593. doi:10.5194/cp-9-2579-2013
- 35 Etheridge, D., Pearman, G.I., Fraser, P.J., 1992. Changes in tropospheric methane
 36 between 1841 and 1978 from a high accumulation-rate Antarctic ice core. *Tellus*
 37 44B, 282–294.
- 38 Faïn, X., Chappellaz, J., Rhodes, R.H., Stowasser, C., Blunier, T., McConnell, J.R.,
 39 Brook, E.J., Preunkert, S., Legrand, M., Debois, T., Romanini, D., 2014. High
 40 resolution measurements of carbon monoxide along a late Holocene Greenland
 41 ice core: evidence for in situ production. *Clim Past* 10, 987–1000. doi:10.5194/cp-
 42 10-987-2014
- 43 Freitag, J., Wilhelms, F., Kipfstuhl, S., 2004. Microstructure-dependent densification of
 44 polar firn derived from X-ray microtomography. *J. Glaciol.* 50, 243–250.
 45 doi:10.3189/172756504781830123



- 1 Fujita, S., Hirabayashi, M., Goto-Azuma, K., Dallmayr, R., Satow, K., Zheng, J., Dahl-
 2 Jensen, D., 2014. Densification of layered firn of the ice sheet at NEEM,
 3 Greenland. *J. Glaciol.* 60, 905–921. doi:10.3189/2014JoG14J006
- 4 Gerland, S., Oerter, H., Kipfstuhl, J., Wilhelms, F., Miller, H., Miners, W.D., 1999.
 5 Density log of a 181 m long ice core from Berkner Island, Antarctica. *Ann.*
 6 *Glaciol.* 29, 215–219. doi:10.3189/172756499781821427
- 7 Gregory, S.A., Albert, M.R., Baker, I., 2014. Impact of physical properties and
 8 accumulation rate on pore close-off in layered firn. *The Cryosphere* 8, 91–105.
 9 doi:10.5194/tc-8-91-2014
- 10 Hörhold, M.W., Kipfstuhl, S., Wilhelms, F., Freitag, J., Frenzel, A., 2011. The
 11 densification of layered polar firn. *J. Geophys. Res.* 116, F01001.
 12 doi:10.1029/2009jf001630
- 13 Hörhold, M.W., Laepple, T., Freitag, J., Bigler, M., Fischer, H., Kipfstuhl, S., 2012. On
 14 the impact of impurities on the densification of polar firn. *Earth Planet. Sci. Lett.*
 15 325–326, 93–99. doi:10.1016/j.epsl.2011.12.022
- 16 Hou, S., Chappellaz, J., Raynaud, D., Masson-Delmotte, V., Jouzel, J., Bousquet, P.,
 17 Hauglustaine, D., 2013. A new Himalayan ice core CH₄ record: possible hints at
 18 the preindustrial latitudinal gradient. *Clim. Past* 9, 2549–2554. doi:10.5194/cp-9-
 19 2549-2013
- 20 Jones, S.J., 1967. Softening of ice crystals by dissolved fluoride ions. *Phys. Lett. A* 25,
 21 366–367. doi:10.1016/0375-9601(67)90702-5
- 22 Keegan, K., Albert, M.R., Baker, I., 2014. The impact of ice layers on gas transport
 23 through firn at the North Greenland Eemian Ice Drilling (NEEM) site, Greenland.
 24 *The Cryosphere* 8, 1801–1806. doi:10.5194/tc-8-1801-2014
- 25 Klein, K., 2014. Variability in dry Antarctic firn—Investigations on spatially distributed
 26 snow and firn samples from Dronning Maud Land, Antarctica. PhD thesis,
 27 University of Bremen, Bremen, Germany.
- 28 MacFarling Meure, C., Etheridge, D., Trudinger, C., Steele, P., Langenfelds, R., van
 29 Ommen, T., Smith, A., Elkins, J., 2006. Law Dome CO₂, CH₄ and N₂O ice core
 30 records extended to 2000 years BP. *Geophys. Res. Lett.* 33,
 31 doi:10.1029/2006GL026152.
- 32 McConnell, J.R., Aristarain, A.J., Banta, J.R., Edwards, P.R., Simões, J.C., 2007. 20th-
 33 Century doubling in dust archived in an Antarctic Peninsula ice core parallels
 34 climate change and desertification in South America. *Proc. Natl. Acad. Sci.* 104,
 35 5743–5748.
- 36 McConnell, J.R., Lamorey, G.W., Lambert, S.W., Taylor, K.C., 2002. Continuous ice-
 37 core chemical analyses using inductively coupled plasma mass spectrometry.
 38 *Environ. Sci. Technol.* 36, 7–11. doi:10.1021/es011088z
- 39 Mitchell, L., Brook, E., Lee, J.E., Buizert, C., Sowers, T., 2013. Constraints on the Late
 40 Holocene anthropogenic contribution to the atmospheric methane budget. *Science*
 41 342, 964–966. doi:10.1126/science.1238920
- 42 Mitchell, L.E., Brook, E.J., Sowers, T., McConnell, J.R., Taylor, K., 2011. Multidecadal
 43 variability of atmospheric methane, 1000–1800 C.E. *J. Geophys. Res.* 116,
 44 doi:10.1029/2010JG001441. doi:10.1029/2010jg001441
- 45 Mitchell, L.E., Buizert, C., Brook, E.J., Breton, D.J., Fegyveresi, J., Baggenstos, D., Orsi,
 46 A., Severinghaus, J., Alley, R.B., Albert, M., Rhodes, R.H., McConnell, J.R.,



- 1 Sigl, M., Maselli, O., Gregory, S., Ahn, J., 2015. Observing and modeling the
2 influence of layering on bubble trapping in polar firn. *J. Geophys. Res.*
3 *Atmospheres* 2014JD022766. doi:10.1002/2014JD022766
- 4 Morville, J., Kassl, S., Chenevier, M., Romanini, D., 2005. Fast, low-noise, mode-by-
5 mode, cavity-enhanced absorption spectroscopy by diode-laser self-locking. *Appl.*
6 *Phys. B Lasers Opt.* 80, 1027–1038.
- 7 Nakamura, T., Jones, S.J., 1970. Softening effect of dissolved hydrogen chloride in ice
8 crystals. *Scr. Metall.* 4, 123–126. doi:10.1016/0036-9748(70)90176-6
- 9 NEEM community members, 2013. Eemian interglacial reconstructed from a Greenland
10 folded ice core. *Nature* 493, 489–494.
- 11 Neftel, A., Oeschger, H., Schwander, J., Stauffer, B., 1983. Carbon dioxide concentration
12 in bubbles of natural cold ice. *J. Phys. Chem.* 87, 4116–4120.
13 doi:10.1021/j100244a025
- 14 NGRIP community members, 2004. High-resolution record of Northern Hemisphere
15 climate extending into the last interglacial period. *Nature* 431, 147–151.
- 16 Orsi, A.J., Kawamura, K., Fegyveresi, J.M., Headly, M.A., Alley, R.B., Severinghaus,
17 J.P., 2015. Differentiating bubble-free layers from melt layers in ice cores using
18 noble gases. *J. Glaciol.* 61, 585–594.
- 19 Priscu, J.C., Hand, K.P., 2010. Microbial habitability of icy worlds. *Microbe Mag. Am.*
20 *Soc. Microbiol.*
- 21 Rasmussen, S.O., Abbott, P.M., Blunier, T., Bourne, A.J., Brook, E., Buchardt, S.L.,
22 Buizert, C., Chappellaz, J., Clausen, H.B., Cook, E., Dahl-Jensen, D., Davies,
23 S.M., Guillevic, M., Kipfstuhl, S., Laepple, T., Seierstad, I.K., Severinghaus, J.P.,
24 Steffensen, J.P., Stowasser, C., Svensson, A., Vallenga, P., Vinther, B.M.,
25 Wilhelms, F., Winstrup, M., 2013. A first chronology for the North Greenland
26 Eemian Ice Drilling (NEEM) ice core. *Clim Past* 9, 2713–2730. doi:10.5194/cp-9-
27 2713-2013
- 28 Rhodes, R.H., Brook, E.J., Chiang, J.C., Blunier, T., Maselli, O.J., McConnell, J.R.,
29 Romanini, D., Severinghaus, J.P., 2015. Enhanced tropical methane production in
30 response to iceberg discharge in the North Atlantic. *Science* 348, 1016–1019.
- 31 Rhodes, R.H., Faïn, X., Stowasser, C., Blunier, T., Chappellaz, J., McConnell, J.R.,
32 Romanini, D., Mitchell, L.E., Brook, E.J., 2013. Continuous methane
33 measurements from a late Holocene Greenland ice core: Atmospheric and in-situ
34 signals. *Earth Planet. Sci. Lett.* 368, 9–19. doi:10.1016/j.epsl.2013.02.034
- 35 Rohde, R.A., Price, P.B., Bay, R.C., Bramall, N.E., 2008. In situ microbial metabolism as
36 a cause of gas anomalies in ice. *Proc. Natl. Acad. Sci.* 105, 8667–8672.
37 doi:10.1073/pnas.0803763105
- 38 Rosen, J.L., Brook, E.J., Severinghaus, J.P., Blunier, T., Mitchell, L.E., Lee, J.E.,
39 Edwards, J.S., Gkinis, V., 2014. An ice core record of near-synchronous global
40 climate changes at the Bølling transition. *Nat. Geosci.* 7, 459–463.
41 doi:10.1038/ngeo2147
- 42 Schwander, J., Barnola, J.M., Andrié, C., Leuenberger, M., Ludin, A., Raynaud, D.,
43 Stauffer, B., 1993. The age of the air in the firn and the ice at Summit, Greenland.
44 *J. Geophys. Res.* 98, 2831–2838. doi:10.1029/92jd02383



- 1 Schwander, J., Sowers, T., Barnola, J.M., Blunier, T., Fuchs, A., Malaizé, B., 1997. Age
2 scale of the air in the summit ice: Implication for glacial-interglacial temperature
3 change. *J. Geophys. Res.* 102, 19483–19493. doi:10.1029/97jd01309
- 4 Sigl, M., Winstrup, M., McConnell, J.R., Welten, K.C., Plunkett, G., Ludlow, F.,
5 Büntgen, U., Caffee, M., Chellman, N., Dahl-Jensen, D., Fischer, H., Kipfstuhl,
6 S., Kostick, C., Maselli, O.J., Mekhaldi, F., Mulvaney, R., Muscheler, R.,
7 Pasteris, D.R., Pilcher, J.R., Salzer, M., Schüpbach, S., Steffensen, J.P., Vinther,
8 B.M., Woodruff, T.E., 2015. Timing and climate forcing of volcanic eruptions for
9 the past 2,500 years. *Nature* 523, 543–549. doi:10.1038/nature14565
- 10 Spahni, R., Schwander, J., Fluckiger, J., Stauffer, B., Chappellaz, J., Raynaud, D., 2003.
11 The attenuation of fast atmospheric CH₄ variations recorded in polar ice cores.
12 *Geophys. Res. Lett.* 30, 1571. doi:10.1029/2003gl017093
- 13 Stowasser, C., Buizert, C., Gkinis, V., Chappellaz, J., Schüpbach, S., Bigler, M., Faïn, X.,
14 Sperlich, P., Baumgartner, M., Schilt, A., Blunier, T., 2012. Continuous
15 measurements of methane mixing ratios from ice cores. *Atmospheric Meas. Tech.*
16 5, 999–1013. doi:10.5194/amt-5-999-2012
- 17 Trudinger, C.M., Enting, I.G., Etheridge, D.M., Francey, R.J., Levchenko, V.A., Steele,
18 L.P., Raynaud, D., Arnaud, L., 1997. Modeling air movement and bubble trapping
19 in firn. *J. Geophys. Res. Atmospheres* 102, 6747–6763. doi:10.1029/96JD03382
- 20 Weiler, K., 2008. On the composition of firn air and its dependence on seasonally varying
21 atmospheric boundary conditions and the firn structure. PhD thesis, University of
22 Bern, Bern, Switzerland.
- 23



- 1 Table 1. Locations, site characteristics and other relevant information for ice cores
 2 featured in this study. Please refer to footnotes for explanation of abbreviations.

Ice core & location (see map Fig. S1)	Depth interval (m)	Gas age interval (yrAD)	Δ age and FWHM (yr)	Accum. rate (cm ice yr ⁻¹)	Mean annual temp. (°C)	Mean liq. cond. (μ S)	Age scale
B40 Dronning Maud Land, E. Antarctica 75.001°S, 0.068°E 2911 m elevation	200–88	331– 1710	811 65	6.8 ^b	-46 ^b	1.33	Ice: ALC+VS Gas: tied to WDC06A-7 ^f
D4 S. Central Greenland 71.40°N, 43.08°W 2,713 m elevation	146–61	1825– 1961	90 14	41	-24	101	Ice: ALC+VS Gas: tied to WDC06A-7 ^f & Law Dome ^g
NEEM NW Greenland 77.45°N, 51.06°W 2,450 m elevation	573–399	-682– 322	187 ^a 17	22 ^c	-28.9 ^c	122	Ice: GICC05 ^h Gas: GICC05 ^h
NGRIP Central Greenland 75.10°N, 42.32°W 2,917 m elevation	569–519	-929– 616	235 18	19 ^d	-31.5 ^d	122	Ice: GICC05 ^h Gas: tied to WDC06A-7 ^f
	254–207	980– 1237				105	
	108–74	1780– 1926				107	
Tunu13 NE Greenland 78.035°N, 33.879°W 2,200 m elevation	213–73	836– 1893	314–369 21–27	10–14	-29 ^c	115	Ice: ALC+VS ⁱ Gas: tied to WDC06A-7 ^f
WAIS Divide West Antarctica 79.47°S, 112.08°W 1766 m elevation	n/a	n/a	208 ^l	20 ^l	-31 ^l	n/a	n/a

3 Footnotes:

4 Δ age = difference between gas age and ice age. If no reference is provided, value is estimated by age scale
 5 synchronisation or OSU firm air model.

6 FWHM= Full Width at Half Maximum of gas age distribution at close-off depth estimated by OSU firm air
 7 model (Rosen et al., 2014).

8 Mean liq. cond. = mean liquid conductivity value for ice core analysed

9 ALC=annual layer count; VS=volcanic synchronisation

10 Gas age scales do not incorporate lock-in zone measurements.

11 References:

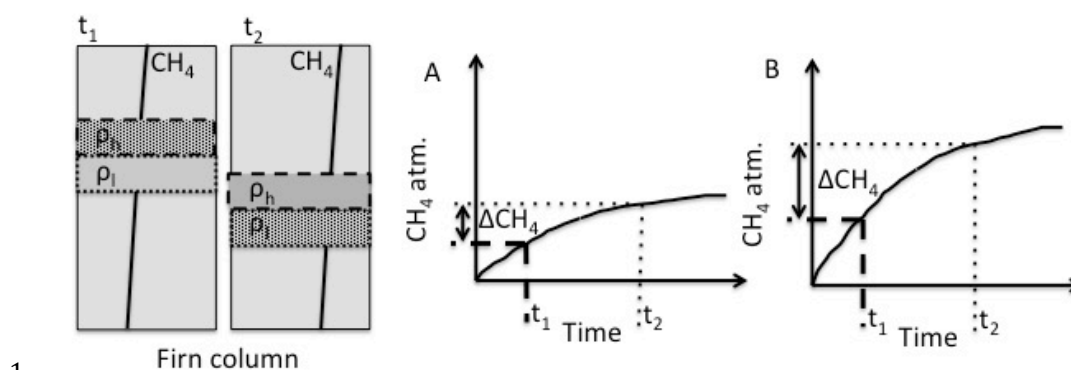
12 a=(Buizert et al., 2014); b=(Klein, 2014); c=(NEEM community members, 2013); d=(NGRIP community
 13 members, 2004); e=(Butler et al., 1999); f=(Mitchell et al., 2013); g=(MacFarling Meure et al., 2006);
 14 h=(Rasmussen et al., 2013); i=(Sigl et al., 2015); j=(Mitchell et al., 2011)



1 Table 2. Discrete CH₄ and total air content measurements on Tunu13 samples containing
 2 melt layers. CH₄ concentrations of the melt layers are estimated based on a simple
 3 mixing calculation using the Summit melt layer value and range stated in the text.
 4 Predicted values are calculated using the assumption that the melt layer was in
 5 equilibrium with the atmosphere, according to Henry's Law (0°C, 0.750 atm.). Henry's
 6 Law constants for CH₄, O₂ and N₂ were obtained from NIST Chemistry WebBook
 7 (webbook.nist.gov). CH₄ concentrations of adjacent samples are used as atmospheric
 8 concentrations at time of melt layer formation. All of these samples are from the Tunu13
 9 Main core.

Sample depth range (m)	Sample CH ₄ conc. (ppb)	Sample total air content (cm ³ /g ice STP)	Melt layer thickness (mm)	Estimated CH ₄ conc. of melt layer (ppb)	x-fold CH ₄ enrichment of ML relative to sample	Mean CH ₄ conc. of adjacent samples (ppb)	Predicted CH ₄ conc. of melt layer in equilib. with atmos. (ppb)
113.910–113.970	773.6	0.0956	4.0	6355 (4781–9940)	8.6	737.1	1492
153.225–153.300	730.3	0.0859	4.0	1829 (1519–2533)	2.5	723.9	1465
156.235–156.285	744.1	0.0941	4.0	5356 (4076–8356)	7.4	721.0	1460
181.710–181.760	700.3	0.0970	4.0	2539 (2020–3721)	3.7	686.1	1389
194.610–194.700	771.9	0.0847	24.0	3683 (2842–5596)	5.4	684.0	1385

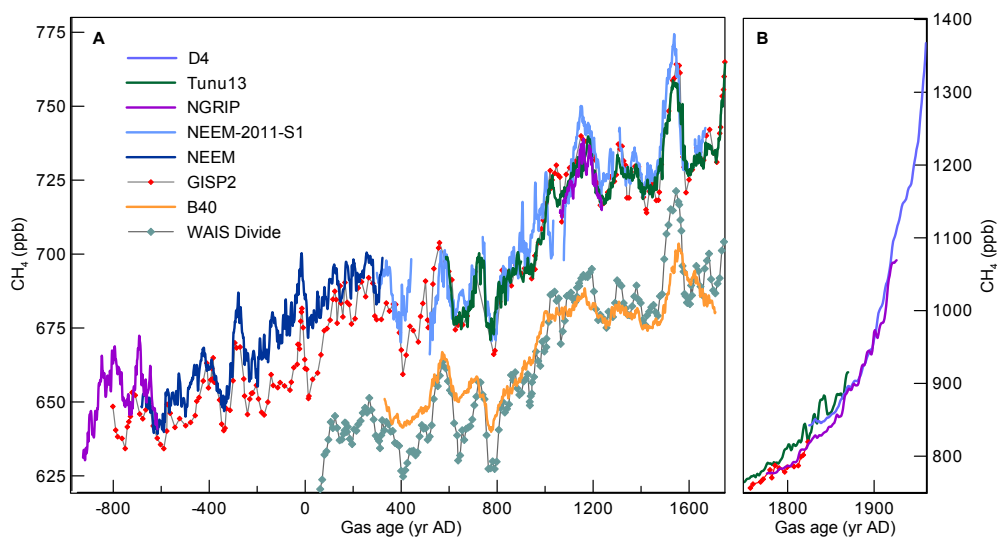
10



1
2 Figure 1.: Schematic to illustrate how the layered bubble trapping mechanism can
3 generate high frequency CH₄ artifacts in ice cores. At time t_1 , air bubbles within the
4 relatively high density (ρ_h) layer are closed off at a relatively shallow depth in the firn
5 column. At time t_2 , air bubbles with the relatively low density (ρ_l) layer are closed off
6 deeper in the firn column. Between t_1 and t_2 the atmospheric concentration of CH₄ is
7 increasing and so the CH₄ concentration in the diffusive column also increases,
8 generating a CH₄ concentration difference ΔCH_4 between the bubbles in depth-adjacent
9 layers trapped at t_1 and t_2 . Increasing the atmospheric CH₄ growth rate (B compared to
10 A) results in a larger ΔCH_4 . A negative atmospheric growth rate would cause a change in
11 the sign of ΔCH_4 .

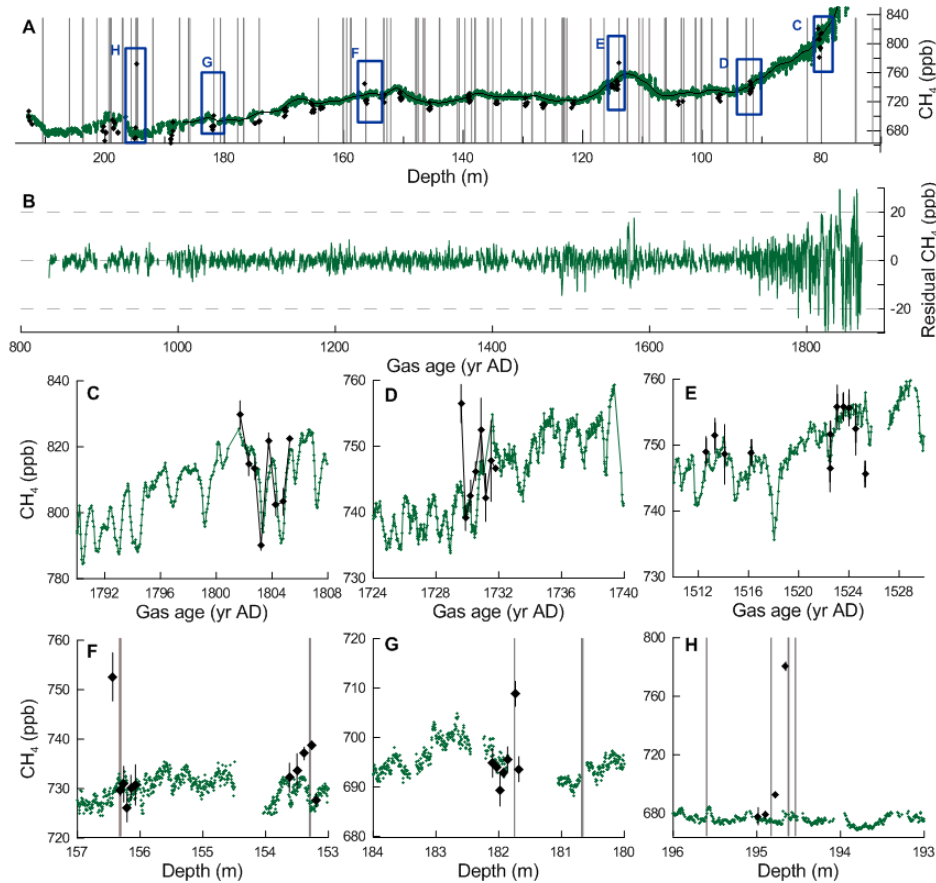


1



2

3 Figure 2. Late Holocene continuous CH₄ data from Tunu13, D4, NGRIP and NEEM
4 Greenland ice cores and B40 Antarctic ice core for time periods -900–1750 AD (A) and
5 1750–1960 AD (B). Each record is a cubic spline fit with 1 yr sample spacing to the 5 s
6 integrated data. No data from the lock-in zone are included on this figure. Also plotted
7 are discrete CH₄ data from GISP2 and WAIS Divide ice cores (Mitchell et al., 2013) and
8 NEEM-2011-S1 continuous CH₄ data (Rhodes et al., 2013).

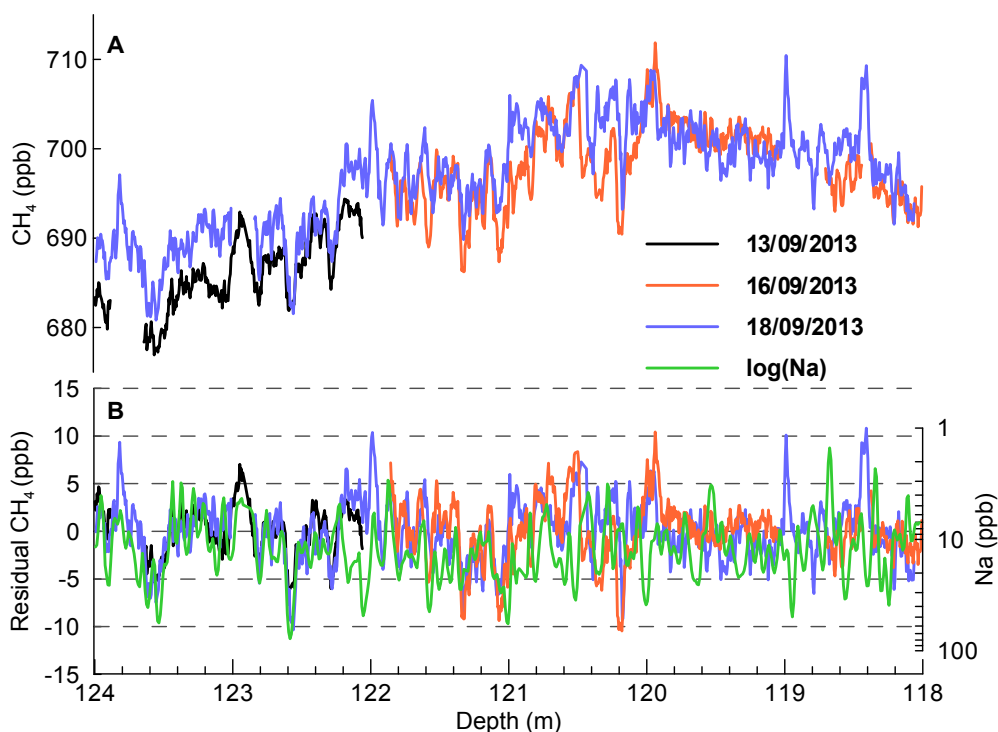


1

2 Figure 3. Decimetre-scale CH₄ variability in Tunu13 mature ice captured by continuous
 3 (green) and discrete (black diamonds) analyses: A) Both records on depth scale with
 4 vertical grey lines indicating depths of bubble-free layers observed; B) Residual high
 5 frequency non-atmospheric component of Tunu13 signal: continuous record from panel
 6 A (green) minus cubic spline fit (black line on panel A). Older data from below 172 m
 7 depth are excluded because there are too many data gaps resulting from poor core quality.
 8 Y-axis has been clipped at -30 and +30 ppb. Data minimum and maximum are -38 and
 9 36 ppb; C, D & E) Zoomed views of high frequency CH₄ variability within blue
 10 rectangles displayed on panel A; F, G & H) Zoomed views of anomalously high discrete
 11 CH₄ concentrations associated with melt layers. CH₄ concentrations of discrete data
 12 points are increased by 8.5 ppb on panels C-H to aid comparison with online data. 2 σ
 13 internal precision uncertainty bars are plotted for discrete data. Horizontal bars on

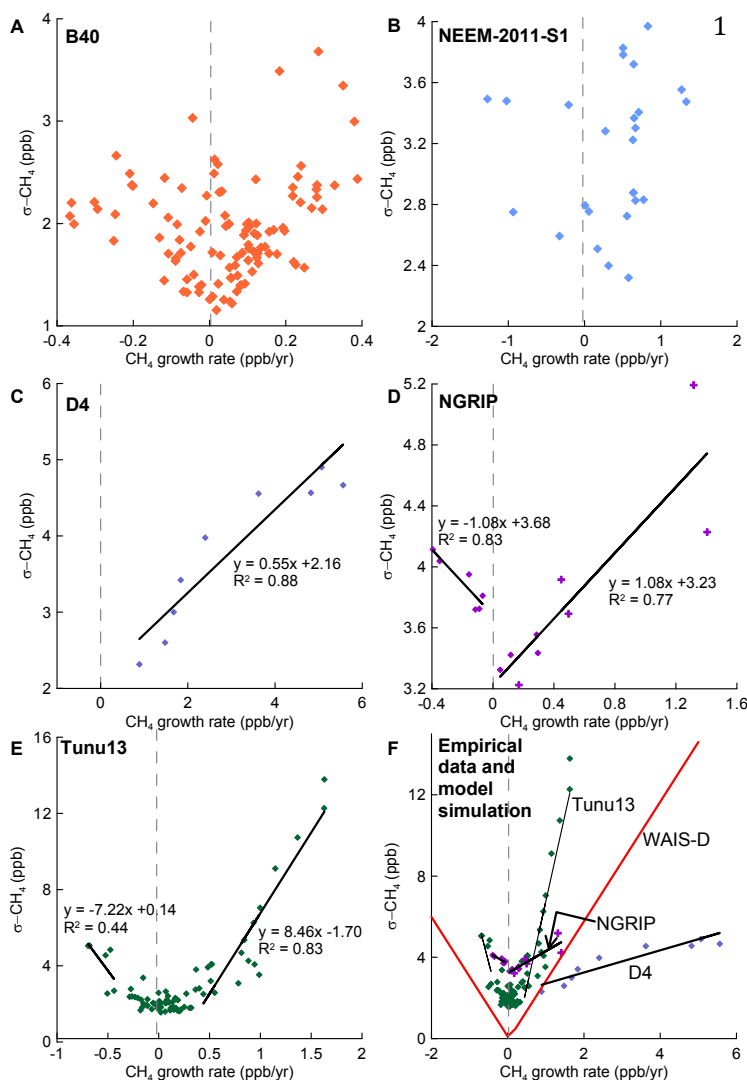


- 1 discrete measurements represent depth interval of each sample. Depth uncertainty for the
- 2 continuous data is estimated to be ± 2 cm (2σ).



1

2 Figure 4. High frequency CH₄ variability in B40 (E. Antarctica) ice. Measured signals
3 (A) and the residual (signal – spline fit) (B) are shown. Variability is replicated by
4 analyses performed on the three dates displayed in legend (dd/mm/yyyy). Gas extraction
5 was performed using a Membrana micromodule degasser on 13/09/2013 and an IDEX in-
6 line degasser on 16/09/2013 and 18/09/2013 (Table S1). Although it is difficult to be
7 certain that anomalously high CH₄ spikes are not the result of ambient air entry at the
8 melterhead, the anomalously low trough cannot be analytical artifacts. Also shown on
9 panel B is Na, which typically co-varies with Cl. Many of the anomalously low CH₄
10 values are coincident in depth with relatively high Na. This depth interval is dated as
11 1493–1583 AD gas age.

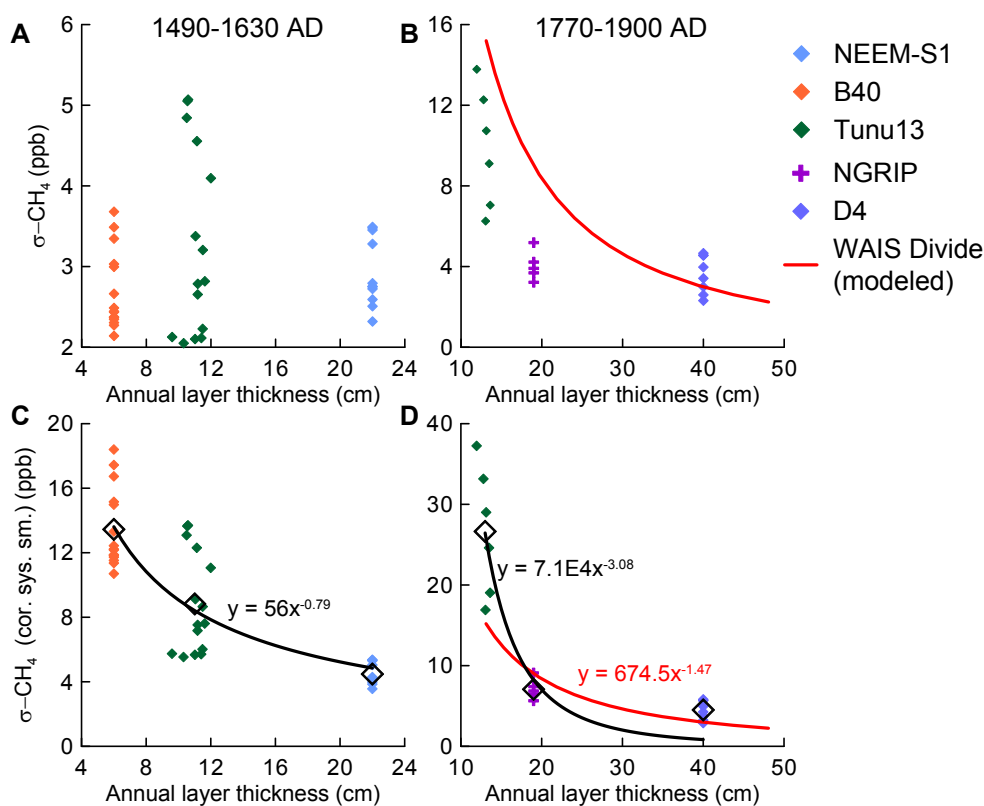


2

3 Figure 5. Relationship between CH₄ growth rate and high frequency CH₄ variability (σ -
 4 CH₄) in the following ice cores: B40 (A), NEEM-2011-S1 (B), D4 (C), NGRIP (D),
 5 Tunu13 (E). σ -CH₄ is calculated every 10 yr for intervals of 40 yr duration (except for 5
 6 NGRIP data points (cross symbols), which are discrete 10 yr intervals with no overlap,
 7 due to poor core quality and discontinuous record). Linear regression of growth rate and
 8 σ -CH₄ is displayed where appropriate. A linear fit is applied to Tunu13 and D4 data with
 9 growth rates $> \pm 0.4$ ppb yr⁻¹ and to NGRIP data with growth rates $> \pm 0.1$ ppb yr⁻¹.



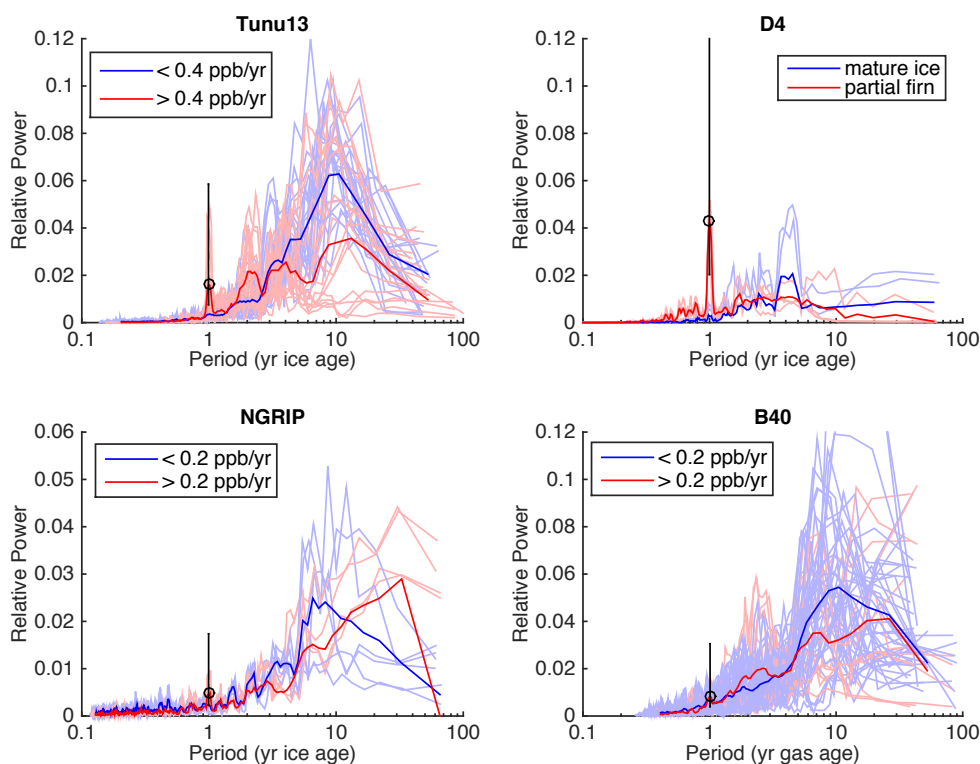
- 1 Panel F displays data from Tunu13, D4 and NGRIP with firn air transport model output
- 2 for the WAIS Divide ice core.
- 3



1

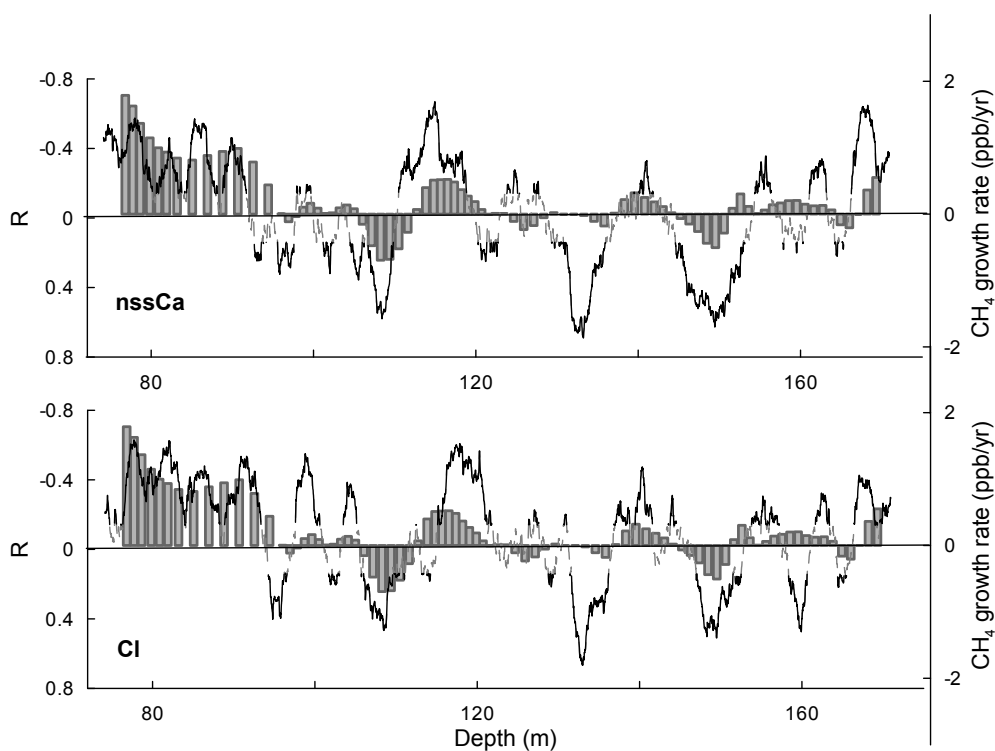
2 Figure 6. Relationship between accumulation rate and high frequency CH₄ variability.
 3 The vertical panels represent two time intervals: 1490–1630 AD (A) and 1770–1900 AD
 4 (B) for which high resolution CH₄ data are available from three ice cores with different
 5 accumulation rates. Note that the three clusters of data points for each time period do not
 6 represent the same ice cores in each case. The top row (A & B) displays CH₄ standard
 7 deviation (σ) about the long-term spline. Values are calculated every 10 yr for intervals
 8 of 40 yr duration as Fig. 5 (except for NGRIP data points on B&D that represent discrete
 9 10 yr intervals). The bottom row (C & D) displays σ -CH₄ values adjusted (increased by
 10 1.25–5 depending on ice core) to correct for the damping effect of the continuous
 11 analytical system (Fig. S2). Mean values for each ice core on each panel are displayed
 12 (black diamonds) with power law relationships (black line). Also shown is the
 13 relationship between accumulation rate and σ -CH₄ for WAIS Divide (at 2.5 ppb yr⁻¹
 14 atmospheric growth rate) as predicted by the CIC firm air transport model.

15



1

2 Figure 7. Multi-taper method (MTM) spectra of high frequency, non-atmospheric
3 residual CH₄ variability of four ice cores. MTM was performed in the ice age domain
4 using 2 tapers and 3 degrees of freedom. Each spectrum represents a 40 yr window of
5 data. For Tunu13, NGRIP and B40 each spectrum is colour-coded according to the CH₄
6 growth rate of that data window. For D4, spectra are colour-coded according to whether
7 or not the time window encompasses data from the lock-in zone (< 82 m depth). All D4
8 spectra represent time windows of CH₄ growth rate > 0.4 ppb yr⁻¹. The bold lines
9 represent averaged spectra for the low/high growth rate or mature ice/partial firn
10 categories. Black open circles represent the mean relative power at 1 yr period. Vertical
11 lines represent 90% confidence intervals for the averaged spectra (bold, red lines only)
12 based on a chi-squared distribution. Spectral peaks are significant for Tunu13 and D4
13 because the confidence interval exceeds the background spectral noise.



1

2 Figure 8. Moving window Spearman's rank correlation between concentrations of non-
3 sea salt (nss) Ca and Cl and σ -CH₄ in the Tunu13 ice core (line) compared to CH₄ growth
4 rate (vertical bars). Note the reverse direction of the left-hand y-axes. Significant ($p <$
5 0.05) (solid line) and non-significant (grey dashed line) coefficient of correlation (R)
6 values are plotted. Correlation is calculated for non-overlapping, 2 m length windows
7 (using 0.5–5 m length windows produces similar results). The σ -CH₄ time series is
8 resampled to the depth spacing of chemistry data (1 cm) so $n = 200$ for each window.